SDU
University of Southern Denmark

Validated 3D finite-element model of the Risso's dolphin (Grampus griseus) head anatomy demonstrates gular sound reception and channelling through the mandibular fats

Wei, Chong; Erbe, Christine; Smith, Adam B.; Yang, Wei Cheng

Published in:
Bioinspiration and Biomimetics

DOI:
10.1088/1748-3190/ad7344

Publication date:
2024

Document version:
Final published version

Document license:
CC BY

Citation for pulished version (APA):
Wei, C., Erbe, C., Smith, A. B., & Yang, W. C. (2024). Validated 3D finite-element model of the Risso's dolphin (Grampus griseus) head anatomy demonstrates gular sound reception and channelling through the mandibular fats. *Bioinspiration and Biomimetics*, *19*(5), Article 056025. https://doi.org/10.1088/1748-3190/ad7344

Go to publication entry in University of Southern Denmark's Research Portal

Terms of use
This work is brought to you by the University of Southern Denmark.
Unless otherwise specified it has been shared according to the terms for self-archiving.
If no other license is stated, these terms apply:

- You may download this work for personal use only.
- You may not further distribute the material or use it for any profit-making activity or commercial gain
- You may freely distribute the URL identifying this open access version

If you believe that this document breaches copyright please contact us providing details and we will investigate your claim.
Please direct all enquiries to puresupport@bib.sdu.dk

Download date: 21. Mar. 2025

Bioinspiration & Biomimetics

PURPOSE-LED PUBLISHING™

PAPER • **OPEN ACCESS**

Validated 3D finite-element model of the Risso's dolphin (*Grampus griseus*) head anatomy demonstrates gular sound reception and channelling through the mandibular fats

To cite this article: Chong Wei *et al* 2024 *Bioinspir. Biomim.* **19** 056025

View the article online for updates and enhancements.

You may also like

- On the spread and decay of wind turbine wakes in ambient turbulence
P B Johnson, C Jonsson, S Achilleos et al.
- Perturbations of the flow induced by a microcapsule in a capillary tube
J Gubspun, C de Loubens, R Trozzo et al.
- Heat flux and upper boundary condition in an open fluidized granular gas
J. J. Brey and M. J. Ruiz-Montero

This content was downloaded from IP address 80.208.71.101 on 16/09/2024 at 12:55

IOP Publishing Bioinspir. Biomim. 19 (2024) 056025 https://doi.org/10.1088/1748-3190/ad7344

Bioinspiration & Biomimetics

CrossMark

OPEN ACCESS

RECEIVED
29 June 2024

REVISED
6 August 2024

ACCEPTED FOR PUBLICATION
23 August 2024

PUBLISHED
4 September 2024

Original content from this work may be used under the terms of the Creative Commons Attribution 4.0 licence.

Any further distribution of this work must maintain attribution to the author(s) and the title of the work, journal citation and DOI.

PAPER

Validated 3D finite-element model of the Risso's dolphin (*Grampus griseus*) head anatomy demonstrates gular sound reception and channelling through the mandibular fats

Chong Wei[1,*], **Christine Erbe**[1], **Adam B Smith**[2] **and Wei-Cheng Yang**[3]

[1] Centre for Marine Science & Technology, Curtin University, GPO Box U1987, Perth, WA 6845, Australia
[2] Marine Research Centre, University of Southern Denmark, 4300 Kerteminde, Denmark
[3] School of Veterinary Medicine, National Taiwan University, Taipei 10617, Taiwan
[*] Author to whom any correspondence should be addressed.

E-mail: chong.wei@curtin.edu.au

Keywords: Risso's dolphin, sound reception, sound production, sound propagation, finite element model, CT scan

Supplementary material for this article is available online

Abstract

Like other odontocetes, Risso's dolphins actively emit clicks and passively listen to the echoes during echolocation. However, the head anatomy of Risso's dolphins differs from that of other odontocetes by a unique vertical cleft along the anterior surface of the forehead and a differently-shaped lower jaw. In this study, 3D finite-element sound reception and production models were constructed based on computed tomography (CT) data of a deceased Risso's dolphin. Our results were verified by finding good agreement with experimental measurements of hearing sensitivity. Moreover, the acoustic pathway for sounds to travel from the seawater into the dolphin's tympanoperiotic complexes (TPCs) was computed. The gular reception mechanism, previously discovered in *Delphinus delphis* and *Ziphius cavirostris*, was also found in this species. The received sound pressure levels and relative displacement at TPC surfaces were compared between the cases with and without the mandibular fats or mandible. The results demonstrate a pronounced wave-guiding role of the mandibular fats and a limited bone-conductor role of the mandible. For sound production modelling, we digitally filled the cleft with neighbouring soft tissues, creating a hypothetical 'cleftless' head. Comparison between sound travelling through a 'cleftless' head vs. an original head indicates that the distinctive cleft plays a limited role in biosonar sound propagation.

1. Introduction

The Risso's dolphin (*Grampus griseus*) is a medium-sized toothed whale found worldwide in temperate and tropical waters (Leatherwood *et al* 1980). Like all toothed whales, they use a set of phonic lips to generate for echolocation, which are then transmitted forward into the water through the forehead (Au 1993). Unlike other toothed whale species, whose foreheads are smooth and round, the Risso's dolphin forehead (including the melon) contains a distinctive vertical cleft, extending from the top of the forehead down to the tip of the rostrum (Leatherwood *et al* 1983). Given its location in the very region where the biosonar beam is projected to the water (Au *et al* 2010, Wei *et al* 2022). It has been speculated that this unique cleft might influence biosonar sound propagation and beam formation in Risso's dolphins (Smith *et al* 2016). Our recent study constructed two-dimensions (2D) finite-element (FE) models based on computed tomography (CT) images of dolphin heads to study the role of the cleft in biosonar beam formation (Wei *et al* 2022). After comparing the hypothetical case (the cleft was filled to make a smooth and round hypothetical forehead) to the original case (an actual Risso's dolphin's forehead with cleft), we found an insignificant role of the cleft in biosonar beam formation. However, our previous study was limited to 2D, in a horizontal slice cut through both the cleft and the right phonic lips, and so, was only able to model a 2D slice of the biosonar beam, whereas odontocete head anatomy collimates projected biosonar clicks into a three-dimensional (3D) beam (Au 1993). Therefore, as the first objective of this study, we present a 3D FE

© 2024 The Author(s). Published by IOP Publishing Ltd

model to further assess any potential role of the cleft in biosonar sound propagation and beam formation.

Odontocete ear complexes, also called tympanoperiotic complexes (TPCs), house two dense, connected bones: the tympanic and periotic bones. These bony ear complexes are wholly or partially decoupled from the skull (Ketten 2000). Bottlenose dolphins (*Tursiops truncatus*) are the best-studied species in regard to sound reception (Brill and Harder 1991, Norris and Harvey 1974, Au *et al* 1998, Møhl *et al* 1999). Early studies based on bottlenose dolphins pointed toward a long-standing 'jaw hearing' notion whereby sound mainly enters via the 'acoustic window' (fat bodies overlying the posterior portions of the lower jaws) and then travels through the jaw and mandibular fats, creating a pathway to the middle ears (Au *et al* 1998). However, sound reception pathways may also vary among species due to variable head anatomy (e.g. different shapes/lengths of the jaws). For example, different from bottlenose dolphins, belugas (*Delphinapterus leucas*) showed sensitivity from both the pan bone regions and the tip of the lower jaw (Mooney *et al* 2008). With a relatively shorter lower jaw, the hearing pathway of Risso's dolphins was different from that of bottlenose dolphins (Mooney *et al* 2015). Furthermore, the 3D finite-difference modelling by Aroyan (2001) on a common dolphin (*Delphinus delphis*) found that the incident sound propagated through and below the pan bones of the lower jaw after entering the dolphin's head: 'Sound incident below the jaw line from forward directions appears to enter the head of this dolphin in the region of the fat deposits forward of the pan bones, to propagate through and below the pan bones of the lower jaw, and to be guided by the left and right mandibular fat bodies back onto the left and right bullae.' Cranford *et al* (2008a) modelling a beaked whale (*Ziphius cavirostris*) also found that the animal received sound through the entire surface of the head like an acoustic antenna. And so, the 'gular' sound reception pathway was proposed. As the second objective of this study, we investigated the existence of gular sound reception in a Risso's dolphin.

Besides various entries and pathways in sound reception among species, studies indicated that regions of sound sensitivity could be frequency-dependent (Popov *et al* 2008). Finless porpoises (*Neophocaena asiaeorientalis asiaeorientalis*) received lower-frequency sounds (8 kHz tones) better from the auditory meatus and higher-frequency sounds (54 kHz and 120 kHz tones and clicks) better from around the jaw tip and mandibular fats regions (Mooney *et al* 2014). Similar evidence was found in bottlenose dolphins and harbour porpoises (*Phocoena phocoena*), in which lower-frequency sounds (below 30 kHz, e.g. communication signals) were received better around the auditory meatus, while higher-frequency sounds were received better through the lower jaw (Norris 1968, Renaud and Popper 1975, Brill *et al* 1988, Kastelein *et al* 1997, Popov *et al* 2008). It remains unclear whether sound reception centres and pathways are also frequency-dependent in Risso's dolphins—the third objective of our study.

Finally, although the notion that various structures (e.g. hollowed mandibles, mandibular fats, and air-filled pterygoid sinus) contribute to sound reception in odontocetes is generally accepted (Norris 1968, Ketten 1992, Aroyan 2001, Cranford *et al* 2008a, Song *et al* 2019, 2023), it is yet undetermined exactly how sound is conducted to the TPCs in most cetaceans including Risso's dolphins (Mooney *et al* 2015). Cranford and Krysl (2015) proposed a bone-conduction mechanism in mysticete sound reception: 'During bone conduction, excitation of the hearing apparatus results from vibrations of the TPC induced by the motion of the skull' (Cranford and Krysl 2015). They suggested that the bone-conduction mechanism was dominant over the pressure mechanism (i.e. sound received through the various soft tissues). However, it was speculated that the bone-conduction mechanism might not be fully applied to odontocete sound reception due to the different anatomy of the TPCs (Cranford and Krysl 2015). Unfortunately, it is relatively challenging to verify this speculation experimentally. Earlier experimental work by Reinwald *et al* (2018) measured elastic waves propagating through the mandible to evaluate the contribution of bone conduction to sound localization. However, the study was based on tests conducted on a dolphin skull (omitted other structures), and did not consider the effects of soft tissues, which are believed to be important contributors to sound reception (Norris 1968, Ketten 1992). Therefore, the fourth objective of our study was to numerically test the bone-conduction hypothesis.

2. Materials and methods

2.1. Medical CT data acquisition and data analysis

An adult, 2.8 m long, male Risso's dolphin was found stranded alive, yet died after rehabilitation. A medical CT scan was performed before necropsy, thus the specimen was fresh, with the head intact. The specimen was scanned in a prone position in a 64-section multidetector CT unit (LightSpeed VCT, GE Healthcare), using 0.625 mm spiral acquisition at 120 kV and 320 mA. Images were formatted in the transaxial plane with a matrix size of 512 × 512 and a field of view of 30 cm × 30 cm. Raw acquisition data and all DICOM images were archived. The DICOM images were imported into Horos™ (Horos Project, Geneva, Switzerland) for analysis and 3D geometrical model reconstruction, as shown in figures 1(A)–(D). During CT data analysis, we first performed 3D

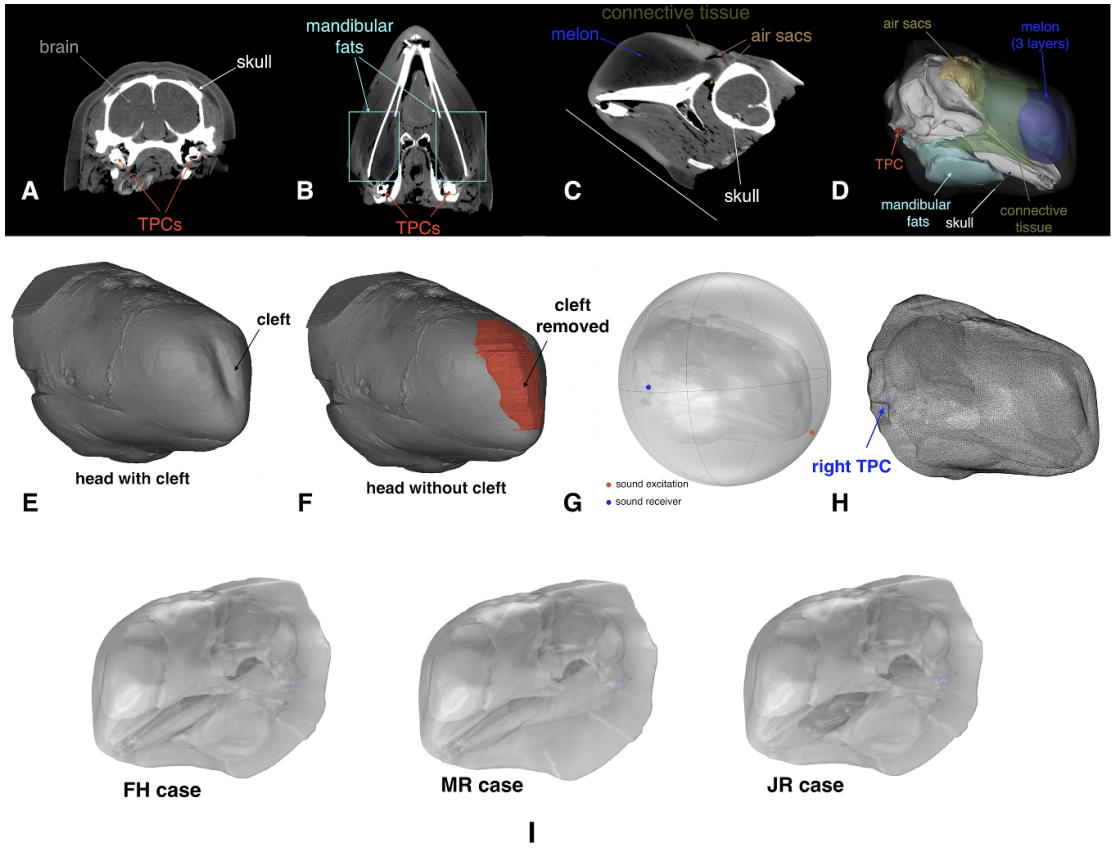

Figure 1. 3D geometry reconstruction and 3D model setup based on high-resolution CT images. (A) Cross plane. (B) Frontal plane. (C) Sagittal plane. (D) 3D reconstruction of the Risso's dolphin's head. The internal structures were constructed in detail, including the TPCs, mandibular fats, connective tissue, melon, skull, musculature, air sacs, etc. (E) The actual Risso's dolphin's head with a distinct cleft along the forehead. (F) The hypothetical head with cleft removed/filled (the red region). (G) The 3D sound reception model setup. (H) Mesh of the clefted head. The blue arrow shows the left TPC. (I) Three sound reception cases: the 'Full head' (FH) case, the 'Mandibular fats removed' (MR) case, and the 'Lower jaw removed' (JR) case.

multiplanar reformation to adjust the head to a natural position (figures 1(A)–(C)). Automatic segmentation was performed for most of the structures based on the difference in Hounsfield unit (HU, a calibrated measure of radio density used in the interpretation of CT images); some of the structures, such as the air sacs, were manually segmented slice by slice. The anatomical configuration of the main structures of the Risso's dolphin, such as the melon (note that the inhomogeneous melon was represented by 3 layers based on different HU values), connective tissue, air sacs, brain, mandibular fats, bony ear/TPCs, and skull were carefully reconstructed (figure 1(D)).

2.2. Tissue acoustic property reconstruction

Unfortunately, the acoustic properties of tissues were not measured for this Risso's dolphin specimen at the time. According to previous studies (Soldevilla *et al* 2005, Wei *et al* 2015), the HU values of the tissues have linear relationships with the tissue properties (i.e. sound speed, density, and acoustic impedance). The HU values of each tissue can be directly obtained from CT data. Based on the HU values, the sound speed and density of the tissues can be converted using the relationships of HU-to-sound-speed and HU-to-density, respectively. This method has been used in previous studies for building FE models of several odontocete species (Wei *et al* 2017, 2018, 2022, 2023); the modelling results matched direct measurements from live, echolocating animals, showing the reliability of this method. In this study, the HU values of the tissues were exported to a text file, which contained the information about coordinates and corresponding HU values. We used the relationships of HU-to-sound-speed and HU-to-density obtained from the previous tissue measurements (Wei *et al* 2015), to convert the HU distributions to the distributions of sound speed and density for the Risso's dolphin. More details can be found in our earlier studies (Wei *et al* 2017, 2018). Then the sound speed and density of the forehead tissues were input according to the acoustic property reconstruction results; the input parameters can be found in our previous study (Wei *et al* 2022).

2.3. FE model construction

Stereolithography files of each tissue generated from 3D reconstruction were imported into COMSOL Multiphysics modelling software (version 6.2; Stockholm, Sweden) for FE analysis (FEA) and corresponding data analysis.

For the sound production modelling, two cases were built to simulate click production and propagation from the head into the seawater: the 'clefted case' and the 'cleftless case'. The clefted case was the head originally imported from the CT data (figure 1(E)), representing an actual Risso's dolphin with a cleft on the forehead. To create the hypothesized 'cleftless' head, we digitally filled the cleft with neighbouring soft tissues, to hypothesize that a Risso's dolphin had a round and smooth forehead as other dolphins (figure 1(F)).

For sound reception modelling, an incident acoustic wave of a given pressure was generated on the surface of the dolphin's head, replicating the methodology of Mooney *et al* (2015) using suction-cup transducers for hearing threshold measurement. The acoustic stimulus, with a frequency of 54 kHz, was moved to seven positions approximately matching the locations where Mooney *et al* (2015) placed their suction-cup transducers. To receive the incident acoustic stimulus from each of the seven positions, a sound reception point was set at the right periotic bone, which contains the cochlea (figure 1(G)). After model validation, the acoustic stimulus was repositioned ahead of the dolphin's head (~10 cm from the tip of the rostrum) and directed toward the head; the location of the stimulus was in the centre to allow sound to travel equally to both ears. To further study the role of the mandibular fats and hollowed mandible/lower jaw in sound reception, two hypothesized cases were created for comparison with the 'full head' case (FH): the 'mandibular fats removed' (MR) and the 'jawbone removed' (JR) cases. In the MR case, the mandibular fats were replaced by the surrounding soft tissues to assume the mandibular fats did not exist; all other structures remained the same (figure 1(I)). In the JR case, the mandible/lower jaw was replaced by the surrounding soft tissues to assume the mandible/lower jaw did not exist, while all other structures remained the same (figure 1(I)). The FH model was based on the actual CT scan data; all structures were included, such as the air sacs, melon, connective tissue, muscle, inner/outer mandibular fats, bony skull, TPCs, and air-filled sinus (figure 1(I)), representing an actual Risso's dolphin's head.

For both sound production and reception models, a water sphere with a diameter of 580 mm was set outside of the dolphin's head to mimic a Risso's dolphin echolocating and receiving sound under water, respectively. A low-reflecting boundary condition (Bérenger 1994) was used for both sound production and reception models at the water sphere. It simulated the acoustic wave propagating in free space with minimal reflections.

COMSOL's free mesher mapped the entire model with the tetrahedral mesh. COMSOL has a built-in detection for small features and narrow regions in a complex geometry. Based on the mesh refinement results, the size of the element was set as a grid spacing of 1/5 of a wavelength λ at the centre frequency f_c of the excitation signal at the source ($\lambda = c_w/f_c$, where c_w is the sound speed in seawater), ensuring the solution had sufficient numeric precision.

A transient time domain FE computation was performed with a time step set at 0.8 μs, allowing detailed temporal description of the high-frequency signal transmission process. The inhomogeneous acoustic wave equation describing the transient acoustic phenomena in the fluid media (e.g. soft tissues, seawater) was solved at each grid point in the model:

$$\frac{1}{\rho_0 c_s^2}\frac{\partial^2 p}{\partial t^2} + \nabla \cdot \left(-\frac{1}{\rho_0}\nabla p\right) = Q \tag{1}$$

where ρ_0 is the equilibrium density (kg m^{-3}), and c_s is the speed of sound (m s^{-1}), $p = (x, t)$ is the sound pressure (Pa) and as such, a function of space x (m) and time t (s), and $Q = Q(x, t)$ is the monopole source locating on the right side of the phonic lips (Madsen *et al* 2013). According to the click characteristics of Risso's dolphin (Philips *et al* 2003, Smith *et al* 2016), a short-duration, broadband pulse with a damped oscillation and a centre frequency of 56 kHz served as the driving force for source excitation (Wei *et al* 2018). It modelled the physical process that the right phonic lips rapidly opened and closed after the airstream passed between them, creating vibration in the associated surrounding soft tissues. Additional details about the sound source setups can be found in Wei *et al* (2022).

When the acoustic waves interact with the solid medium, such as the skull and TPC bone, the longitudinal and transverse waves can be described as:

$$\rho\frac{\partial^2 \boldsymbol{u}}{\partial^2 t} = (\lambda + 2\mu)\nabla(\nabla \cdot \boldsymbol{u}) - \mu\nabla \times (\nabla \times \boldsymbol{u}) \tag{2}$$

where $\boldsymbol{u}$ is the position vector, λ and μ are two Lame constants, characterizing compression and shear modulus in the solid medium, respectively (Urick 1983). For fluid–solid boundaries, the boundary condition includes the following interaction between fluid and solid domains:

$$\boldsymbol{F} = -\boldsymbol{n}_s p \tag{3}$$

$$-\boldsymbol{n}_a \cdot \left(-\frac{1}{\rho_0}\nabla p\right) = \boldsymbol{a}_n \tag{4}$$

where $\boldsymbol{F}$ is a pressure load (force per unit area) on the boundaries where the fluid interacts with the solid, $\boldsymbol{n}_s$ is the outward-pointing unit normal vector seen from inside the solid domain, $\boldsymbol{n}_a$ is the outward-pointing unit normal vector seen from inside the liquid, and $\boldsymbol{a}_n$ is normal acceleration of the solid surface in the liquid domain boundary. The Young's modulus of the skull and TPC bones was set as 19 GPa and 30 GPa,

respectively (Currey 1979, Tubelli *et al* 2012, Cranford and Krysl 2015). The Poisson's ratio was set as 0.3, a value commonly used for bone (Currey 1979, Tubelli *et al* 2014).

3. Results

3.1. Sound reception modelling

Figure 2 shows the hearing thresholds measured by Mooney *et al* (2015) from a Risso's dolphin using a jawphone stimulus to elicit auditory evoked potentials (AEPs). In our sound reception models, the acoustic stimulus with the frequency of 54 kHz was excited at approximately the same stimulus locations used in Mooney *et al* (2015). The acoustic energy attenuated while the sound travelled through the head structures, resulting in a transmission loss. For each location, the transmission loss to the right ear was calculated by the difference in sound pressure level (SPL) from the surfaces of the head to the right ear. Figure 2 shows the magnitude of transmission loss to the right ear for each location. A significantly higher transmission loss (least sensitive) was found when sound arrived from the forehead. The most sensitive regions were found at three locations (light green dots): the tip of the lower jaw, the midline region of the lower jaw (gular), and above the mandibular fats. Our simulation results match the hearing measurement results of Mooney *et al* (2015), suggesting the reliability of this sound reception model.

Based on the verified sound reception model, an incident acoustic wave (40 kHz) was incident directly from the front of the head (figure 1(G)), then interacted with the internal anatomical structures. Five instances of the sound pressure field as the sound wave travelling through were captured, as shown in figure 3. The sound wave entered from the tip of the head, travelled through the gular/throat region before reaching the mandibular fats (vertical view in figure 3(A)). Figure 3(B) (horizonal view) shows that the sound wave propagated along the mandibles and was channelled by the mandibular fats to the TPCs. The results indicated a 'gular pathway' in Risso's dolphin sound reception, which was first suggested in the common dolphin and beaked whale (Aroyan 2001, Cranford *et al* 2008a). The results also supported the direct hearing sensitivity measurements by Mooney *et al* (2015).

The dorsal branches of the inner mandibular fats are connected to TPCs through numerous ligaments (figure 4). When acoustic waves with higher frequencies (32 kHz in figure 4(B) and 40 kHz in figure 4(C)) were channelled through the terminals of the inner mandibular fats, significantly higher amplitudes of the acoustic pressure were observed at the TPCs, suggesting that more acoustic energy was directed and focused to the surfaces of the TPCs through the mandibular fats. By contrast, such acoustic pressure distribution was not found when the lower-frequency sound (2 kHz) was received. The results suggest that the Risso's dolphin might receive higher-frequency sounds (e.g. >30 kHz) primarily through the mandibular fats regions, which is similar to experiment data from finless porpoises, bottlenose dolphins, and harbour porpoises from previous studies (Norris 1968, Renaud and Popper 1975, Brill *et al* 1988, Kastelein *et al* 1997, Popov *et al* 2008, Mooney *et al* 2014).

When only the mandibular fats (both inner and outer mandibular fats) were removed from the head (MF case), received SPLs at the periotic bone surfaces were reduced across all tested frequencies (2–40 kHz) compared to the FH case (figure 5(A)). The SPLs of two cases were only close in the lower frequencies (2–3 kHz). The average SPL across all frequencies for the FH case was 166.1 dB, which was higher than that of the MR case (163.8 dB). The results indicate that a higher SPL was received at the ears when the mandibular fats were present, suggesting the mandibular fats played a role of guiding the acoustic energy along the lower jaw to the ears.

When only the lower jaw was removed from the head (JR case), the average relative displacement of all frequencies for the FH case was 2.45×10^{-6} mm, which was close to that of the JR case (2.46×10^{-6} mm). There were no obvious trends in change of displacement throughout all frequencies (figure 5(B)), suggesting an insignificant role of the lower jaw in carrying the motion/vibration to the ear bone complexes.

3.2. Sound production and propagation modelling: the role of the cleft

Figures 6(A)–(C) display the three instants in time when an echolocation click was generated by the phonic lips and then propagated through the forehead in the 'clefted' and 'cleftless' cases. After click generation at the phonic lips, the signals were reflected by the surrounding air sacs and then propagated towards the forehead structures. Figure 6(A) shows the instant when the clicks were about to enter the dense connective tissues in the two cases. Subsequently, the clicks were travelling through the melon inside of the head before reaching the cleft region (figure 6(B)). The sound pressure fields of the two cases were identical till this moment since the forehead structures along this sound propagation pathway were the same in both cases.

While the clicks were passing through the cleft region (figure 6(C)), the sound waves were slightly bent on the surface of the 'clefted' head due to the existence of the cleft. The detailed comparison of forehead sound propagation in the two cases can be found as an animation in supplementary file (S1). We also modelled the 3D pattern of outgoing beam formation between the two cases at the instant when the

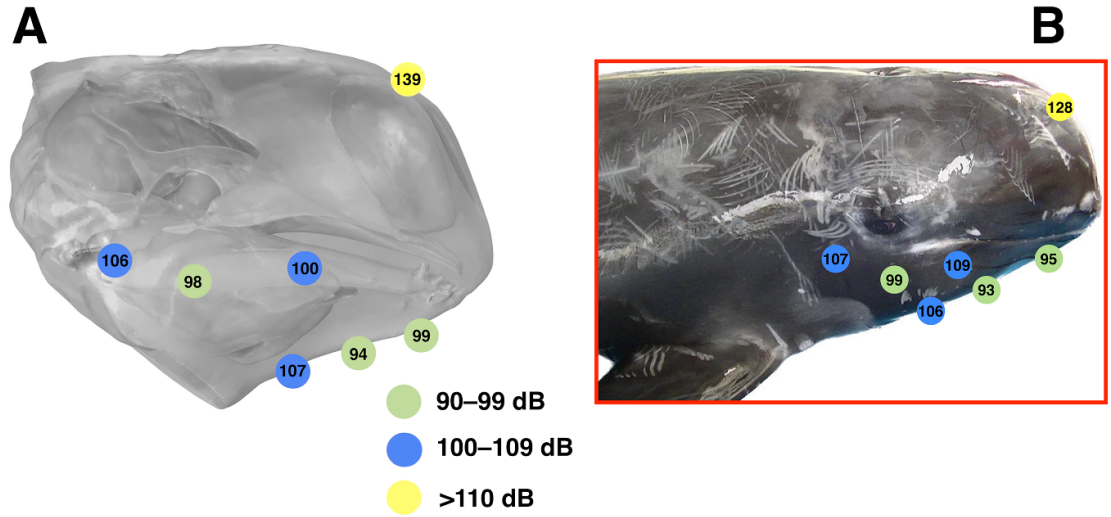

Figure 2. Comparison of the transmission loss to the right ear between the simulation and measurements. Our simulation results are on the left (A). Measurements by Mooney *et al* (2015) are shown in the red box on the right. More information can be found in Mooney *et al* (2015) (B). Colour dots indicate sensitivity ranges. The numbers in circles give the auditory sensitivity in dB re 1 μPa. Lower numbers indicate more sensitive hearing locations. Note that the anatomy on the left is slightly rotated from the anatomy displayed on the right and the slight differences in the morphology of the two individuals.

clicks reached the water spheres and were radiating in to surrounding seawater as shown in figure 6(D). Notably, the beam patterns of the two cases were nearly identical. To explore the impact of the bending in the forehead sound propagation (figure 6(C)), we quantified differences in the individual waveform of the produced click at three different locations: the centre of the forehead cleft (Point C, red dot in figure 6(C)), the tip of the rostrum (Point T, black dot in figure 6(C)) and ∼10 cm in front of the head (Point F, blue dot in figure 6(C)) for both clefted and cleftless cases. The outgoing signals passing through these three points were exported for comparison. Figure 6(E) shows that the waveforms of clicks transmitted to Points C, T and F in both cases were similar. The correlation coefficients of the signals at Points C, T, and F between the two cases were 0.99, 0.99 and 0.99, respectively, indicating that the presence of the cleft had a minimal effect on the temporal and amplitude patterns of the projected click wave oscillations. The results from our 3D models were consistent with the 2D FE model by Wei *et al* (2022) and suggested that the presence of the forehead cleft has a minimal impact on the formation patterns of outgoing echolocation signals on the surface of the Risso's dolphin head as they propagate into the water.

4. Discussion

We developed CT-based FE sound reception models to investigate the sound reception pathway and the roles of the mandibular fats and mandible/jawbone in sound reception. The TPCs house the middle and inner ears; in particular, the periotic bones contain the cochlea. The exact acoustic modes of propagation from the mandibular fats into each cochlea are still poorly understood. Therefore, we set the periotic bones as the sound receivers in our models.

The FEA results demonstrate that sounds were received by the entire surface of the Risso's dolphin's head. As the sound waves pass through the anatomical structures of the head, the dense bony skull and associated air spaces (e.g. nasal passages, pterygoid sinus, peribullary sinus, etc) function as the acoustic shields to prevent the received sound from propagating to the TPCs through the upper head (and also shield the TPCs from self-generated sounds by the phonic lips). Therefore, sounds were channelled to the TPCs by the lower head structures following the gular reception pathway (Norris 1968, Aroyan 2001, Cranford *et al* 2008a), a sound reception mechanism that was also found in other odontocetes, such as *Delphinus delphis* and *Ziphius cavirostris* (Aroyan 2001, Cranford *et al* 2008a). Our simulated sound reception pathway also agrees well with the hearing sensitivity measurement results from Mooney *et al* (2015) using AEP; in fact, the gular reception mechanism may apply to all odontocetes.

Previous modelling results by Cranford and Krysl (2015) suggested that mysticetes might receive sounds primarily by bone conduction mechanism since the periotic bones of the mysticetes are firmly attached to the skull. According to the bone conduction theory (Cranford and Krysl 2015), the incident pressure creates a force to drive the periotic bones into motion directly through the skull. The tympanic and periotic bones are connected through relatively flexible bony pedicles. Therefore, the tympanic bones will be forced to follow the motion of the periotic bones. As an odontocete, the ear anatomy of the Risso's dolphin is different from the mysticetes (figures 1(A) and (B)), as numerous ligaments hold the TPCs in

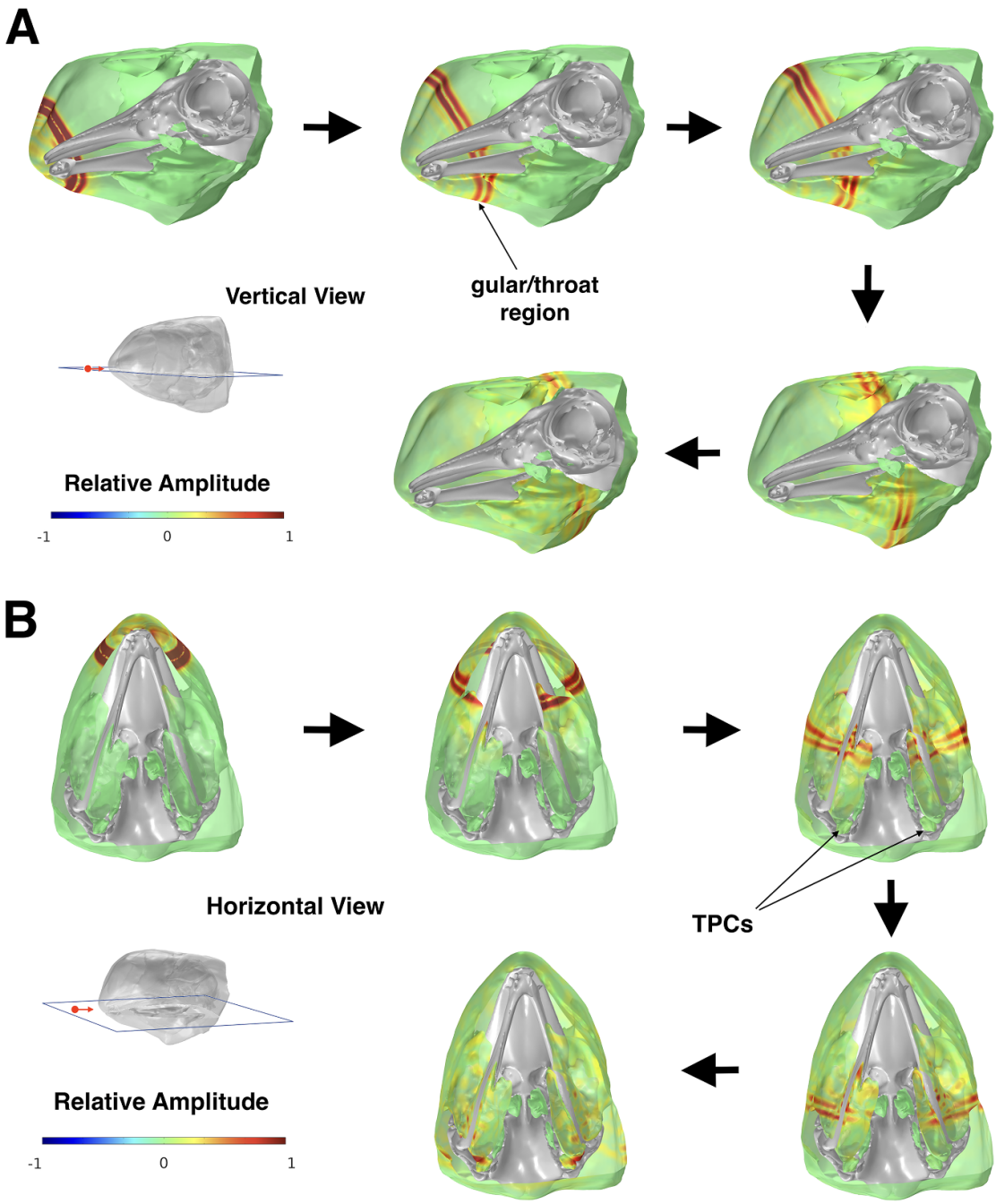

Figure 3. Sound reception through the internal structures. To better visualize the sound reception pathway through the internal structures, the vertical (A) and horizontal (B) views are displayed by adding clip planes through the head. The red dots and red arrows denote the location of the sound source and the direction of the incident sound, respectively. The left side of the head is removed in the vertical view and the lower part of the head is removed in the horizontal view, respectively.

a foam-filled cavity outside the skull (Ketten 2000). With the separation between the periotic bones and the skull, only limited motion can be directly carried to the TPCs via the skull which is likely the reason there are no pronounced effects on the received displacement after removing the mandible (figure 5(B)). Instead, the TPCs of the Risso's dolphin are connected to the dorsal branches of the inner mandibular fats, creating a lower impedance channel for acoustic energy being guided through the fatty soft tissues (The mandibular fats also play a role in impedance matching. Further analysis can be found in supplementary file S2). Missing the mandibular fats (figure 5(A)) would result in reducing the acoustic energy received at the ears.

Early anatomic work based on a *Ziphius cavirostris* surmised that the air-filled pterygoid sinus might act as sound mirror to focus sounds at specific locations on the sound reception pathway and might also provide acoustic isolation for the TPCs (Cranford *et al* 2008b). In our FE sound reception models, because of the impedance mismatch, we also observed reflection to a certain extent from the air-filled sinus as sound waves travelled through the lower jaw region

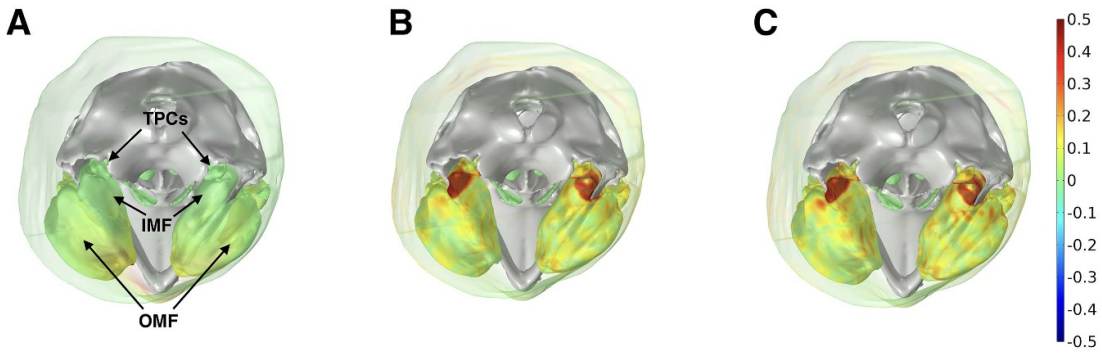

Figure 4. Comparison of the received sound pressure from the mandibular fats terminal to the TPCs between three incident sound frequencies. (A) 2 kHz, (B) 32 kHz, and (C) 40 kHz. The sound pressure was relative to the highest sound pressure in the 40 kHz case. For display purposes, the muscles were highly transparent. Note that the sound pressure field in the 2 kHz case was amplified 3 times for clarity. IMF, inner mandibular fats; OMF, outer mandibular fats.

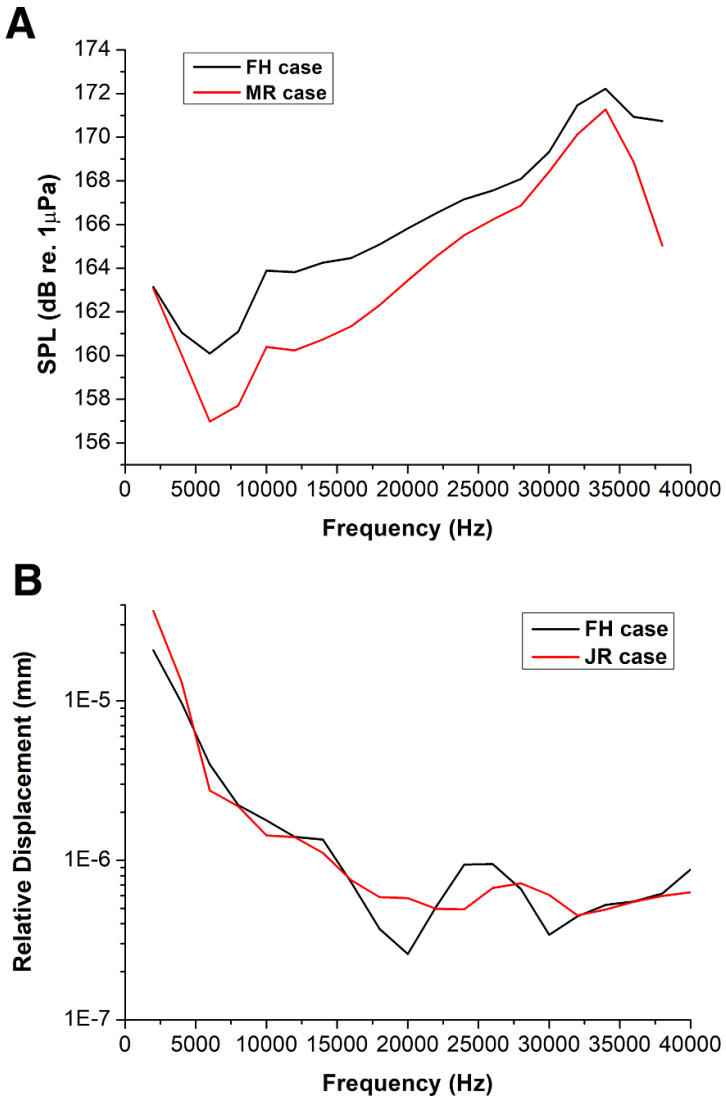

Figure 5. Comparison of the received SPL and displacement at periotic bone surfaces among different cases. (A) Received SPL at periotic bone surfaces comparing the FH case to the MR case. (B) Relative displacement at periotic bones comparing the FH case to the JR case.

of the Risso's dolphin. We built a hypothesized FE model by removing these air spaces associated with TPCs to create an 'Air space removed' (AR) case. The comparison results between the AR and the FH cases only showed a minor effect on the received SPLs at the TPCs. This is likely due to the air spaces of

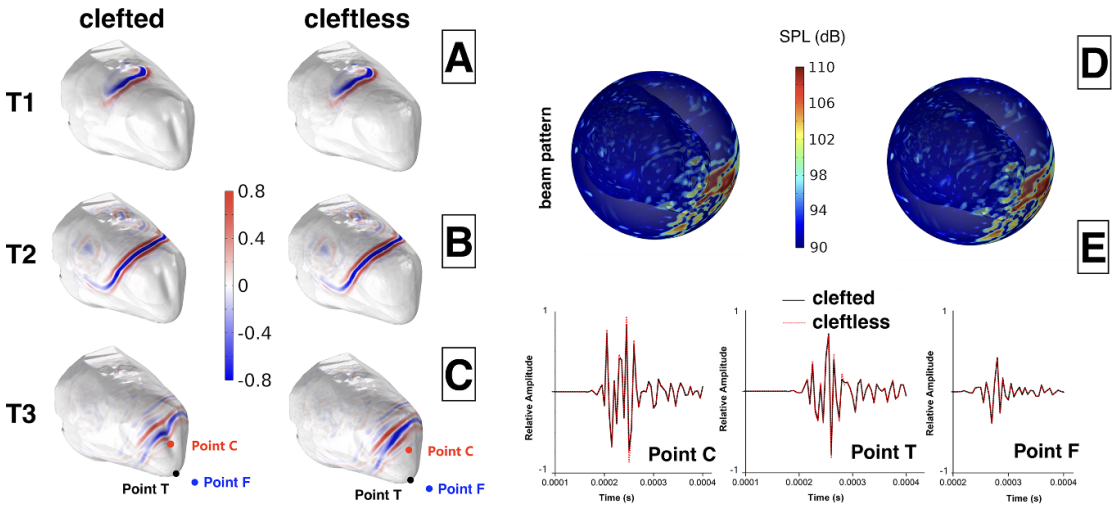

Figure 6. Comparisons of sound propagation through the forehead at three instances in time (T1, T2, T3) and the beam pattern on the water sphere between the 'clefted' and 'cleftless' cases. (A) T1: After the clicks were generated at the phonic lips. (B) T2: When sound waves were about to reach the cleft region. (C) T3: When the sound waves were passing through the forehead cleft. (D) Beam patterns when the sound waves were reaching the water spheres. The colour bar denotes the scale of relative sound pressure for the sound pressure field and SPL for the beam pattern, respectively. The sound pressure was relative to the highest sound pressure value at T3. (E) Outgoing signals at Point C, Points T and F. The black solid lines represent the signals exported from the 'clefted' case and the red dashed lines represent the signals exported from the 'cleftless' case. Amplitudes of all waveforms scaled relative to the highest amplitude (Point C).

this Risso's dolphin specimen being partially inflated in our CT data. The reconstructed pterygoid sinus on the left side was split into several small pieces. The air volumes of the air spaces on the two sides were also clearly asymmetrical. Thus, the shapes of the air spaces might be different from a live animal. Therefore, we decided to only focus on studying the roles of the mandible and mandibular fats rather than jumping to conclusions based on the partially inflated air-filled sinus of our models. Addressing the role of the air-filled pterygoid sinus in sound reception for Risso's dolphins would be important future work when a better specimen is available.

Our previous work developed 2D CT-based FE models (slices cut through the phonic lips and cleft in the vertical and horizontal planes, respectively) to determine the potential effects of the cleft on the resultant beam (Wei *et al* 2022). 2D modelling only represents approximations based on one of the major slices, but sound propagation through the forehead cleft is a 3D manner (the shapes of the outgoing beam and the cleft are both in 3D); moreover, sound spreads circularly in a 2D model but spreads spherically in a 3D model. Therefore, the 3D modelling from this study represents a better methodology for further examining the role of the cleft. Our 3D modelling results also suggest a limited role of the forehead cleft in the biosonar sound propagation of the Risso's dolphin's head, showing a high degree of agreement with the previous 2D modelling results.

It should be noted that 3D FE modelling requires massive computation costs. During our mesh refinement tests, we found that our 384 GB RAM workstation can only efficiently calculate the model with the number of degrees of freedom no more than 7.5 million. Because of this limited computing power of our current workstation, we only examined sound reception pathway up to 40 kHz and generated a click with a centre frequency of 56 kHz in the sound production model. This constraint also restricted us to calculating only the near-field beam pattern shown in figure 6(D). According to Philips *et al* (2003), the average centre frequency of echolocation clicks emitted by the Risso's dolphin was 56.5 kHz, with a maximum centre frequency reaching 85.7 kHz. Therefore, our FE sound production model primarily represents the transmission of lower-frequency clicks (below 56 kHz) through the cleft. Upgrading the workstation to investigate the role of the cleft in in higher-frequency sound propagation (above 56 kHz) would be the logical follow-on to this research. Moreover, the developed 3D sound production model will assist in research regarding sound production and propagation mechanisms in Risso's dolphins. For example, the model can be expanded to investigate the dynamic beam steering mechanisms of Risso's dolphins as more experimental data becomes available in the future.

5. Conclusions

We constructed 3D numerical models based on CT data of a Risso's dolphin to simulate the sound reception and sound propagation processes in the head. The FE model revealed the sound reception pathway through the lower head structures, mainly through the gular/throat region, supporting the gular reception mechanism previously discovered in *Delphinus*

delphis and *Ziphius cavirostris*, which may also apply to other odontocetes. The FEA results also demonstrate a significant wave-guide role of the mandibular fats but a limited bone conduction role of the mandible. Furthermore, after upgrading our methodology from previous 2D modelling to current 3D modelling, the potential effects of the forehead cleft on the resultant beam are still found to be minor. In general, this study led to a better understanding of the sound reception and propagation processes that occurred inside the head of the Risso's dolphin.

Data availability statement

All data that support the findings of this study are included within the article (and any supplementary files).

Acknowledgments

Chong Wei is supported by a Fellowship from the Forrest Research Foundation. We thank Lachlan G Gill and Leander Erbe King from Curtin University for helping with the modelling. We wish to thank Dr James L Aroyan for the discussion about the sound reception modelling.

ORCID iDs

Chong Wei https://orcid.org/0000-0002-2359-9285
Christine Erbe https://orcid.org/0000-0002-7884-9907

References

Aroyan J L 2001 Three-dimensional modeling of hearing in *Delphinus delphis J. Acoust. Soc. Am.* **110** 3305–18
Au W W L 1993 *The Sonar of Dolphins* (Springer) p 277
Au W W L, Houser D S, Finneran J J, Lee W, Talmadge L A and Moore P W 2010 The acoustic field on the forehead of echolocating Atlantic bottlenose dolphins (*Tursiops truncatus*) *J. Acoust. Soc. Am.* **128** 1426–1413
Au W W L, Mohl B, Nachtigall P E, Pawloski J and Aroyan J 1998 Acoustic pathways of hearing in the bottlenose dolphin, *Tursiops truncatus J. Acoust. Soc. Am.* **103** 2908
Bérenger J P 1994 A perfectly matched layer for the absorption of electromagnetic waves *J. Comput. Phys.* **114** 185–200
Brill R L and Harder P J 1991 The effects of attenuating returning echolocation signals at the lower jaw of a dolphin (*Tursiops truncatus*) *J. Acoust. Soc. Am.* **89** 2851–7
Brill R L, Sevenich M L, Sullivan T J, Sustman J D and Witt R E 1988 Behavioural evidence for hearing through the lower jaw by an echolocating dolphin (*Tursiops truncatus*) *Mar. Mammal. Sci.* **4** 223–30
Cranford T W and Krysl P 2015 Fin whale sound reception mechanisms: skull vibration enables low-frequency hearing *PLoS One* **10** e0116222
Cranford T W, Krysl P and Hildebrand J A 2008a Acoustic pathways revealed: simulated sound transmission and reception in Cuvier's beaked whale (*Ziphius cavirostris*) *Bioinsp. Biomim.* **3** e016001
Cranford T W, McKenna M F, Soldevilla M S, Wiggins S M, Shadwick R E, Krysl P, St Leger J A and Hildebrand J A 2008b Anatomic geometry of sound transmission and reception in Cuvier's beaked whale (*Ziphius cavirostris*) *Anat. Rec.* **291** 353–78
Currey J D 1979 Mechanical properties of bone tissues with greatly differing functions *J. Biomech.* **12** 313–9
Kastelein R, van der Kaay L S P, Staal C, Schooneman N M and van Ligtenberg C L 1997 Detection of bone conductor signals by a harbour porpoise (*Phocoena phocoena*) *The Biology of the Harbour Porpoise* ed A J Read, P R Wiepkema and P Nachtigall (De Spil Publishers) pp 313–27
Ketten D R 1992 The marine mammal ear: specializations for aquatic audition and echolocation *The Evolutionary Biology of Hearing* ed D B Webster, R J Fay and A N Popper (Springer) pp 717–50
Ketten D R 2000 Cetacean ears *Hearing by Whales and Dolphins* ed W W L Au, A N Popper and R R Fay (Springer) pp 43–108
Leatherwood S, Perrin W F, Kirby V L, Hubbs C L and Dahleim M 1980 Distribution and movements of Risso's dolphin. *Grampus griseus*, in the Eastern North Pacific *Fish. Bull.* **77** 951–63 (available at: https://swfsc-publications.fisheries.noaa.gov/publications/CR/1980/8048.PDF)
Leatherwood S, Reeves R R and Foster L 1983 *The Sierra Club Handbook of Whales and Dolphins* (Tien Wah Press) pp 226–9
Madsen P T, Lammers M, Winsniewaska D and Beedholm K 2013 Nasal sound production in echolocating delphinids (*Tursiops truncatus* and *Pseudorca crassidens*) is dynamic, but unilateral: clicking on the right side and whistling on the left side *J. Exp. Biol.* **216** 4091–102
Møhl B, Wwl A, Pawloski J L and Nachtigall P E 1999 Dolphin hearing: relative sensitivity as a function of point of application of a contact sound source in the jaw and head region *J. Acoust. Soc. Am.* **105** 3421–4
Mooney T A, Li S, Ketten D R, Wang K and Wang D 2014 Hearing pathways in the Yangtze finless porpoise, *Neophocaena asiaeorientalis asiaeorientalis J. Exp. Biol.* **217** 444–52
Mooney T A, Nachtigall P E, Castellote M, Taylor K A, Pacini A F and Esteban J-A 2008 Hearing pathways and directional sensitivity of the beluga whale, *Delphinapterus leucas J. Exp. Mar. Biol. Ecol.* **362** 108–16
Mooney T A, Yang W C, Yu H Y, Ketten D R and Jen I F 2015 Hearing abilities and sound reception of broadband sounds in an adult Risso's dolphin (*Grampus griseus*) *J. Comp. Physiol.* A **201** 751–61
Norris K S 1968 The evolution of acoustic mechanisms in odontocete cetaceans *Evolution and Environment* ed E T Drake (Yale University Press) pp 297–324
Norris K S and Harvey G W 1974 Sound transmission in the porpoise head *J. Acoust. Soc. Am.* **56** 659–64
Philips J D, Nachtigall P E, Au W W L, Pawloski J L and Roitblat H L 2003 Echolocation in the Risso's dolphin. *Grampus griseus J. Acoust. Soc. Am.* **113** 605–16
Popov V V, Supin A Y, Klishin V O, Tarakanov M B and Pletenko M G 2008 Evidence for double acoustic windows in the dolphin, *Tursiops truncatus J. Acoust. Soc. Am.* **123** 552–60
Reinwald M, Grimal Q, Marchal J, Catheline S and Boschi L 2018 Bone-conducted sound in a dolphin's mandible: experimental investigation of elastic waves mediating information on sound source position *J. Acoust. Soc. Am.* **144** 2213–24
Renaud D L and Popper A N 1975 Sound localization by the bottlenose porpoise *Tursiops truncatus J. Exp. Biol.* **63** 569–85
Smith A B, Kloepper L N, Yang W-C, Huang W-H, Jen I-F, Rideout B P and Nachtigall P E 2016 Transmission beam characteristics of a Risso's dolphin (*Grampus griseus*) *J. Acoust. Soc. Am.* **139** 53–62
Soldevilla M S, McKenna M F, Wiggins S M, Shadwick R E, Cranford T W and Hildebrand J A 2005 Cuvier's beaked whale (*Ziphius cavirostris*) head tissues: physical properties and CT imaging *J. Exp. Biol.* **208** 2319–32
Song Z, Ou W, Li J, Zhang C, Fu W, Xiang W, Wang D, Wang K and Zhang Y 2023 Sound reception in the Yangtze finless

porpoise and its extension to a biomimetic receptor *Biomimetics* **15 8** 366
Song Z, Zhang Y, Mooney T A, Wang X, Smith A B and Xu X 2019 Investigation on acoustic reception pathways in finless porpoise (*Neophocaena asiaorientalis sunameri*) with insight into an alternative pathway *Bioinspir. Biomim.* **14** 016004
Tubelli A A, Zosuls A, Ketten D R and Mountain D C 2014 Elastic modulus of cetacean auditory ossicles *Anatom. Rec.* **297** 892–900
Tubelli A A, Zosuls A, Ketten D R, Yamato M and Mountain D C 2012 A prediction of the minke whale (*Balaenoptera acutorostrata*) middle-ear transfer function *J. Acoust. Soc. Am.* **132** 3263–72
Urick R J 1983 *Principles of Underwater Sound* 3rd edn (McGraw-Hill)
Wei C, Au W W L, Ketten D R, Song Z and Zhang Y 2017 Biosonar signal propagation in the harbor porpoise's (*Phocoena phocoena*) head: the role of various structures in the formation of the vertical beam *J. Acoust. Soc. Am.* **141** 4179–87
Wei C, Au W W L, Ketten D R and Zhang Y 2018 Finite element simulation of broadband biosonar signal propagation in the near- and far-field of an echolocating Atlantic bottlenose dolphin (*Tursiops truncatus*) *J. Acoust. Soc. Am.* **143** 2611–20
Wei C, Gill L G, Erbe C, Smith A B and Yang W-C 2022 The distinctive forehead cleft of the Risso's dolphin (*Grampus griseus*) hardly affects biosonar beam formation *Animals* **12** 3472
Wei C, Houser D, Erbe C, Mátrai E, Ketten D R and Finneran J J 2023 Does rotation increase the acoustic field of view? Comparative models based on CT data of a live dolphin versus a dead dolphin *Bioinspir. Biomim.* **18** 035006
Wei C, Wang Z, Song Z, Wang K, Wang D, Au W W L and Zhang Y 2015 Acoustic property reconstruction of a neonate Yangtze finless porpoise's (*Neophocaena asiaeorientalis*) head based on CT imaging *PLoS One* **10** e0121442